Journal of Visualized Experiments

Time-lapse Imaging of Neuronal Arborization Using Sparse Adeno-associated Virus Labeling of Genetically Targeted Retinal Cell Populations

--Manuscript Draft--

Article Type:	Invited Methods Collection - JoVE Produced Video
Manuscript Number:	JoVE62308R1
Full Title:	Time-lapse Imaging of Neuronal Arborization Using Sparse Adeno-associated Virus Labeling of Genetically Targeted Retinal Cell Populations
Corresponding Author:	Samantha Ing-Esteves The Hospital for Sick Children Toronto, Ontario CANADA
Corresponding Author's Institution:	The Hospital for Sick Children
Corresponding Author E-Mail:	samantha.esteves@mail.utoronto.ca
Order of Authors:	Samantha Ing-Esteves
	Julie Lefebvre
Additional Information:	
Question	**Response**
Please specify the section of the submitted manuscript.	Neuroscience
Please indicate whether this article will be Standard Access or Open Access.	Standard Access (US$2,400)
Please indicate the **city, state/province, and country** where this article will be **filmed**. Please do not use abbreviations.	Toronto, Ontario, Canada
Please confirm that you have read and agree to the terms and conditions of the author license agreement that applies below:	I agree to the Author License Agreement
Please provide any comments to the journal here.	

TITLE:

Time-lapse Imaging of Neuronal Arborization Using Sparse Adeno-associated Virus Labeling of Genetically Targeted Retinal Cell Populations

AUTHORS AND AFFILIATIONS:

Samantha Ing-Esteves[1,2], Julie L. Lefebvre[1,2]

[1]Program for Neuroscience and Mental Health, Hospital for Sick Children, Toronto, Ontario, Canada

[2]Department of Molecular Genetics, University of Toronto, Toronto, Ontario, Canada

Email Address of Co-author:

Samantha Ing-Esteves (samantha.esteves@mail.utoronto.ca)

Corresponding Author:

Julie L. Lefebvre (Julie.Lefebvre@sickkids.ca)

KEYWORDS

Live-cell imaging, morphogenesis, dendrite development, intravitreal injections, Cre-Lox, Adeno-associated virus, deconvolution, starburst amacrine cells

SUMMARY:

Here, we present a method for investigating neurite morphogenesis in postnatal mouse retinal explants by time-lapse confocal microscopy. We describe an approach for sparse labeling and acquisition of retinal cell types and their fine processes using recombinant adeno-associated virus vectors that express membrane-targeted fluorescent proteins in a *Cre*-dependent manner.

ABSTRACT:

Discovering mechanisms that pattern dendritic arbors requires methods to visualize, image, and analyze dendrites during development. The mouse retina is a powerful model system for the investigation of cell type-specific mechanisms of neuronal morphogenesis and connectivity. The organization and composition of retinal subtypes are well-defined, and genetic tools are available to access specific types during development. Many retinal cell types also constrain their dendrites and/or axons to narrow layers, which facilitates time-lapse imaging. Mouse retina explant cultures are well suited for live-cell imaging using confocal or multiphoton microscopy, but methods optimized for imaging dendrite dynamics with temporal and structural resolution are lacking. Presented here is a method to sparsely label and image the development of specific retinal populations marked by the Cre-Lox system. Commercially available adeno-associated viruses (AAVs) used here expressed membrane-targeted fluorescent proteins in a Cre-dependent manner. Intraocular delivery of AAVs in neonatal mice produces fluorescent labeling of targeted cell types by 4–5 days post-injection (dpi). The membrane fluorescent signals are detectable by confocal imaging and resolve fine branch structures and dynamics. High-quality videos spanning 2–4 h are acquired from imaging retinal flat-mounts perfused with oxygenated artificial cerebrospinal fluid (aCSF). Also provided is an image postprocessing pipeline for dendrite deconvolution and three-dimensional (3D) drift correction.

This protocol can be used to capture several cellular behaviors in the intact retina and to identify novel factors controlling neurite morphogenesis. Many developmental strategies learned in the retina will be relevant for understanding the formation of neural circuits elsewhere in the central nervous system.

INTRODUCTION:

Dendrites of retinal neurons form intricate, yet specific, patterns that influence their function within neural circuits. In the vertebrate retina, diverse types of retinal ganglion cells (RGCs) and amacrine cell interneurons bear unique dendritic morphologies that differ in arbor size, location, branch length, and density[1]. During postnatal development, RGCs and amacrine cells extend exuberant dendritic processes into a neuropil called the inner plexiform layer (IPL), where they receive bipolar cell inputs transmitting photoreceptor signals[2]. As captured by time-lapse imaging of fluorescently labelled retinal populations in chick or zebrafish larvae, dendrite morphogenesis is highly dynamic[3–5]. Within days, dendritic arbors expand, remodel, and ramify to narrow sublayers of the IPL, where they synapse with select partners. The arbors exhibit different structural dynamics over development, with changes in relative rates of branch addition, retraction, and stabilization. Amacrine and RGC dendrites also exhibit different outgrowth and remodeling behaviors that might reflect type-specific arborization. However, these studies tracked broad amacrine or RGC populations and focused on laminar targeting, which is just one aspect of morphology.

The mechanisms that produce the vast morphological diversity observed across retinal subtypes are poorly understood. The objective of this group was to develop a method to capture dendrite dynamics and arbor remodeling of defined retinal subtypes in mice. Identifying cell type-specific mechanisms of dendrite patterning requires methods to visualize and measure dendrite behaviors of cells of interest. Organotypic cultures of mouse retinas are well suited for live-cell imaging studies using confocal or multiphoton microscopy. Developing retinas are dissected and mounted into a flat explant that can be imaged for several hours in a recording chamber or cultured over a few days with limited effects on the circuitry[6,7]. Live retinal neurons can be labeled by a variety of techniques, including dye-filling by electrodes, electroporation, biolistic delivery of particles coated with lipophilic dyes or plasmids encoding fluorescent proteins (e.g., Gene Gun), as well as genetically encoded cell labels[7–10]. However, these approaches are inefficient for imaging dendrite dynamics of specific retinal subtypes. For instance, dye-filling methods are low-throughput and require electrophysiology apparatus and additional genetic labels to reliably target cells of interest. Moreover, the strong fluorescence signals in the soma can obscure nearby dendrites.

Biolistic gene delivery methods can simultaneously label dozens of cells, but steps involving high-pressure particle delivery and overnight incubation of isolated retina can compromise cell physiology and dendritic outgrowth. This paper proposes that recent genetic tools can be employed to capture early dendrite dynamics with cell type and structural resolution, given the following experimental criteria. First, to resolve the fine branches and filopodia that dominate developing arbors, the method should label neurons with bright, fluorescent proteins that fill processes in the entire arbor. The fluorescence labeling should not fade due to photobleaching

during the imaging period. A variety of fluorescent protein variants have been generated and compared for suitability for in vivo/ex vivo imaging[11] based on brightness and photostability. Second, the fluorescent proteins (XFPs) must be expressed at sufficiently high levels by the earliest stage of dendrite morphogenesis, so that the narrow developmental window is not missed. In analyses of static timepoints in the mouse retina, dendrite development occurs during the first postnatal week and includes phases of outgrowth, remodeling, and stabilization[10,12–15]. Third, the method should lead to selective labelling or to an increased probability of labelling of the neuronal subpopulation of interest. Although RGC and amacrine subtypes can be distinguished by their mature morphological characteristics and IPL stratification patterns[16–20], the challenge is to identify subtypes during development based on immature structures. This task is facilitated by the expansion of transgenic tools to label specific retinal cell types during development.

Transgenic and knock-in mouse lines in which cellular and temporal expression of fluorescent proteins or Cre is determined by gene regulatory elements are widely used to study retinal cell types[13,21–23]. Key observations on subtype-specific patterns of dendrite development have come from studies of transgenic mouse retinas at static timepoints[10,14,24,25]. The Cre-Lox system, in particular, enables exquisite gene manipulation and monitoring of subtypes using a variety of recombinase-dependent reporters, sensors, and optogenetic activators. These tools have led to discoveries of subtype-specific molecular programs and functional properties that underlie retinal circuit assembly[26–30]. However, they have yet to be leveraged to study subtype-specific dendrite dynamics in the mouse retina. Fourth, labelling of the target subpopulation must be sufficiently sparse so that the entire neuronal arbor can be identified and traced. Low-density labeling can be achieved by combining Cre mouse lines with transgenes introduced by electroporation or by recombinant AAVs. If available, tamoxifen-inducible Cre lines or intersectional genetic strategies can also be used. Finally, the cell should be labelled in a minimally invasive manner and imaged using acquisition parameters so as not to compromise the tissue or interfere with cellular function required for dendrite morphogenesis.

Presented here is a method to apply transgenic tools and confocal microscopy to investigate dendrite dynamics in live mouse retinal explants. Cre transgenic mouse lines have been combined with AAV vectors that express fluorescent proteins upon Cre recombination, which allows for sparse labeling of retinal cells of interest. Commercially available AAVs are delivered to neonatal retina by intravitreal injections. This paper demonstrates that AAVs produce significantly high and cell type-specific fluorescent expression by 4 dpi, allowing access to postnatal time points. To illustrate this approach, the cholinergic “starburst” amacrine interneuron was labelled by delivering Brainbow AAV in neonatal mice expressing the choline acetyltransferase (ChAT)-internal ribosome entry site (IRES)-Cre transgene, which is active in the early postnatal retina[31,32]. Starburst amacrine cells develop a stereotyped and radial arbor morphology that is shaped by dendrite self-avoidance mediated by the clustered protocadherins[33,34]. This paper shows that the resolution of starburst dendrites and filopodia is significantly improved by the tethering of XFPs to the plasma membrane with the addition of the CAAX motif which undergoes farnesylation, as used for the Brainbow AAVs[31]. Finally, time-lapse imaging parameters have been provided along with image postprocessing that produce

high-quality images amenable for dendrite reconstruction and morphometric quantification. This protocol can be used to identify factors controlling dendrite morphogenesis and to capture several cellular behaviors in the intact retina.

PROTOCOL:

NOTE: This protocol spans 2 days with a minimum period of 4–5 days for viral transduction between experimental days (**Figure 1A**). Animal experiments are performed in accordance with the Canadian Council on Animal Care Guidelines for Use of Animals in Research and Laboratory Animal Care under protocols approved by the Laboratory of Animal Services Animal Use and Care Committee at the Hospital for Sick Children (Toronto, Canada).

1. Preparations for the neonatal AAV injections and imaging experiments

1.1. Select a Cre mouse line to label the retinal cell populations of interest. Confirm Cre recombinase expression at the time of AAV injections by crossing to a Cre transgenic reporter or through immunostaining with a Cre antibody.

1.2. Breed transgenic Cre mice (8–16 weeks old) to generate Cre-positive neonatal animals.

NOTE: For this demonstration, ChAT-IRES-Cre knock-in mice were used to target the cholinergic Starburst amacrine cells.

1.3. Obtain recombinase-dependent AAV virus encoding fluorescent protein(s). For optimal labeling of fine processes, select vectors that express modified XFPs targeting the plasma membrane.

NOTE: This study used the Brainbow virus (BBV), AAV9.hEF1a.lox.TagBFP.lox.eYFP.lox.WPRE.hGH-InvBYF and AAV9.hEF1a.lox.mCherry.lox.mTFP1.lox.WPRE, which provide the option for multicolour labeling (**Figure 1B**). Farnesylated enhanced yellow fluorescent protein (eYFP) and monomeric Cherry (mCherry) expression produced the strongest fluorescent signals for live imaging. A single BBV can be used to image individual arbors, while co-injection of BBVs can be used to label more cells or neighboring arbors with distinct fluorophores. If using multiple fluorescent proteins, ensure minimal emission spectrum overlap (**Figure 1C**). Microscope acquisition parameters must be adjusted to capture distinct XFP signals.

1.4. Prepare ~1–3 µL aliquots of AAVs in individual low-binding tubes for single-use stocks to avoid freeze/thaw cycles. Store at -80 °C.

1.5. Prepare borosilicate glass micropipettes with very fine tips using a micropipette puller.

NOTE: Puller settings vary depending on filament and puller being used; see **Figure 2A** for final tip size and shape. Typical droplet diameters are 600 µm.

1.6. Obtain a microinjection system and associated tubing. Connect the microinjector to a pressurized **air** port.

[Place **Figure 1** here]

2. Intravitreal injections of AAVs in neonatal mice

2.1. Thaw an AAV aliquot on ice. Prepare a ~1:4 AAV dilution using sterile saline or phosphate-buffered saline. Prepare ~0.5 µL of AAV dilution per animal (~0.25 µL per eye) in case the micropipette breaks, and a new pipette needs to be filled. Store the remaining undiluted AAV at 4 °C, and use within 2 weeks.

NOTE: In this experiment, the supplier AAV concentration was ~1-2 × 10^{13} genome content (GC)/mL and diluted to a final concentration of 4 × 10^{12} GC/mL. Optimize the viral concentration to obtain the desired labeling density.

2.2. To visualize the injections, add approximately 1 µL of 0.02% Fast Green FCF dye solution for every 15 µL of AAV dilution to color the solution blue.

2.3. Transfer a mouse cage with dam and newborn litter (postnatal day (P) 0.5–3) to a procedure room with microinjection equipment. Keep the animals in the same cage with nests and bedding to minimize maternal stress and rejection of pups.

2.4. Sterilize the injection area with 70% ethanol, and place sterile diaper pads on bench surfaces. Prepare a warm platform (e.g., a heating pad) for recovery from hypothermia-induced anesthesia.

2.5. Backfill the micropipette with the AAV dilution using a microsyringe. Under a stereomicroscope, break the micropipette tip with a 30 G needle to unseal the tip.

NOTE: **Figure 2A** shows the backfilled tip—both sealed (top) and unsealed (middle).

2.6. Anesthetize neonatal mice by hypothermia by placing 1–2 animals on ice. Once the animal no longer moves in response to paw pinch (~2 min), place the animal under a stereomicroscope. If desired, tattoo paw pads with tattoo ink and 30 G needle, and collect tail clippings for DNA isolation to identify animals by genotyping.

2.7. Swab the skin overlying the eyes with 70% ethanol. Use a 30 G needle to open the fused eyelid (**Figure 2B**). Apply light pressure with the fingers to open the eye, and poke a small hole through the cornea at the cornea-sclera junction (**Figure 2C**).

2.8. Insert the glass micropipette into the hole, and press the microinjector foot pedal 2–4 times to inject the AAV into the intravitreal space. Slowly remove the micropipette, and confirm AAV injection by visualizing blue dye through the pupil **(Figure 2D).**

NOTE: With an ejection pressure of 6–8 psi and pulse time of 600–800 ms, a 600 µm diameter droplet is ejected (**Figure 2A, bottom**). Approximately 0.23–0.45 µL of AAV solution is injected per eye. Blue solution outside the eye indicates that the AAV was not injected into the eye. Blue solution leaking from the injection site indicates that the AAV may have leaked out, reducing transfection efficiency.

2.9. Gently press the eyelids together to re-seal, and place the pup onto a heated pad. Once the animals recover a pinkish color and are responsive, gently transfer them back to the housing cage.

2.10. Repeat the injection procedure for the remaining animals in the litter. Allow a minimum of 4–5 days for viral transduction before imaging the retina.

[Place **Figure 2** here]

3. Retinal dissections for imaging experiment

3.1. Prepare retinal aCSF (119 mM NaCl, 2.5 mM KCl, 1.3 mM $MgCl_2 \cdot 6H_2O$, 2.5 mM $CaCl_2 \cdot 2H_2O$, 1 mM NaH_2PO_4, 11 mM glucose, and 20 mM 4-(2-hydroxyethyl)-1-piperazineethanesulfonic acid (HEPES free acid)[35]. If desired, prepare and freeze 10x solution; thaw and dilute to 1x as needed.

3.2. Oxygenate the retinal aCSF by bubbling with carbogen (95% O_2, 5% CO_2) for a minimum of 15 min. Adjust the pH to 7.4. Keep in a sealed container until use to ensure that the aCSF remains oxygenated.

NOTE: Retinas require a high concentration of O_2. It is important to keep aCSF oxygenated throughout the experiment.

3.3. Embed a 60 mm diameter Petri dish into an ice tray (fashion an ice tray out of lab plastic, e.g., a pipette box lid), and place it under a stereomicroscope. Fill the Petri dish with oxygenated retinal aCSF.

3.4. Euthanize mice P9 and younger by decapitation. Euthanize mice P10 and older by isoflurane induction, or an alternate method approved under the animal protocol, followed by decapitation.

3.5. If the eyelids are sealed, cut the eyelid flap to expose the eye. Use forceps to enucleate the eyes, and transfer them into the cold retinal aCSF from step 3.3.

3.6. To dissect the retinal cup, under a stereomicroscope (magnification 25x), stabilize the eye by clasping the optic nerve using a Dumont #5 forcep (**Figure 3A**).

3.7. Poke a hole in the center of the cornea with a 30 G needle, and then insert one tip of the microscissors into the hole to make an incision from the hole to the end of the cornea. Repeat to make 4 slices in the cardinal directions, creating 4 “flaps” (**Figure 3A**).

3.8. With two Dumont #5 forceps, grasp and pull the two adjacent flaps apart, gently peeling the sclera from the retina. Repeat with the remaining cornea flaps, and remove the sclera from the retina (**Figure 3B**).

3.9. Remove the lens from the retinal cup using the forceps. With microscissors, make 4 radial incisions from the edge of the retina towards the optic nerve, creating 4 equal petals (**Figure 3B**). Repeat steps 3.4–3.7 for the second eye.

4. Retinal flat-mount preparation

4.1. Prepare grey mixed cellulose ester (MCE) membrane filter discs for mounting. If using large diameter MCE membrane filters, cut the disc into quadrants (roughly 1 cm across). Place the MCE disc onto the center of a larger white filter paper (**Figure 3D).**

NOTE: MCE filters are also available in 1 cm diameter discs. The MCE filter disc must be large enough to fit 1–2 retinas, but small enough to fit into the imaging chamber. As MCE membranes hold a static charge, minimize contact and handling of the MCE membrane.

4.2. Handling retinas using two size 3/0 paint brushes, flip one retinal cup onto a paintbrush with the retinal ganglion cell side down. Gently lift the retina out of the aCSF, making sure the water tension does not tear the retina (**Figure 3C**).

4.3. While still holding the paintbrush with the retina, use a transfer pipette to place a droplet of aCSF in the center of the MCE filter paper (**Figure 3C**, right). Float the retina into the droplet of aCSF created by the surface tension. Use paint brushes to position the retina RGC side up within the droplet and to unfold the four petals.

4.4. Once positioned, create a water bridge between the paintbrush and white filter paper to break the surface tension of the droplet.

NOTE: When aCSF is wicked away, the retina will adhere to the MCE filter paper (**Figure 3D,E**). Flat-mounted retinas can be handled by grasping the MCE disc with forceps. If the aCSF droplet quickly wicks away prior to forming a water bridge, this may indicate that the MCE membrane is not charged. Use a fresh MCE membrane, and minimize the time between enucleation and imaging by dissecting and flat-mounting retinas immediately before moving retinas into the imaging chamber.

[Place **Figure 3** here]

5. Time-lapse confocal imaging of live whole-mount retina preparations

5.1. Assemble the live-imaging incubation chamber for an upright confocal microscope as seen in **Figure 4.**

NOTE: For inverted confocal systems, flat-mounts are placed RGC side down directly onto the glass bottom coverslip of the incubation chamber. Once the retinas make contact with the coverslip, they cannot be moved.

5.2. Fill the chamber with oxygenated aCSF, and turn on the pump and temperature controller (temperature 32–34 °C, flow rate 1 mL/min). Do not allow temperature to rise above 34 °C.

5.3. To transfer the retinal flat-mount to the perfusion chamber, stop the pump, and remove the aCSF that is in the chamber. Place the MCE disc with the retinal flat-mount into the (empty) incubation chamber.

5.4. Place a sample weight onto the flat-mount; pre-wet the weight to break surface tension. Refill the chamber with the warmed aCSF, and circulate aCSF at ~1 mL/min.

5.5. Position the nosepiece with the 25x water dipping objective (numerical aperture 0.95) into the imaging chamber. Screen for labelled cells of interest using epifluorescent light **(Figure 4C)**.

5.6. Adjust the imaging volume to capture dendritic features of interest.

NOTE: This study captured the complete dendritic arbor at 1024 x 1024 pixels per frame, z-step 1 µm, and a frame rate of 2 min between each z-stack. Final image sizes are ~100 µm x 100 µm x 20 µm.

5.7. To adjust the laser power to an optimal setting, use a look-up table that identifies both oversaturated and undersaturated pixels. While scanning, adjust the laser power such that no pixels are oversaturated (i.e., at an intensity of 255 or above). Continue imaging as long as required, or until the there is a significant and detectable decline in fluorescent signal and increase in noise (typically 2–4 h).

NOTE: Reduced laser power is recommended as deconvolution algorithms work optimally when pixels are distributed over the full dynamic range. Pixel intensity should not exceed 254; empirical analyses of neurites revealed that pixel values below 170 are ideal for deconvolution. Fast scan speeds (400–600 Hz) with line averaging (2–3) are preferable to single, slower scans of the same total pixel dwell timeThe area of prolonged imaging often photobleaches, but other explant sections remain viable. Multiple regions in a flat-mount can be imaged, each for 2–4 h, with a total incubation time of 6 hours. Imaging sessions beyond 6 h have not been systematically tested. Neurite degradation and blebbing are signs that the explant viability is declining.

5.8. After imaging, fix the retinal flat-mounts and membrane filter with cold 4% paraformaldehyde for 1–2 h at 4 °C. Amplify the fluorescent labels in the fixed retinas by immunohistochemistry for further analyses.

NOTE: Post-imaging fixation is not possible when using an inverted confocal; retinas are not removable without destroying the tissue.

[Place **Figure 4** here]

6. Image deconvolution and post-processing in ImageJ

6.1. Import the image series, split the series by time, and color if it is a multi-color image. Ensure that all time points for one color are contained in the same folder.

NOTE: Import Bio-formats if using ImageJ (Bio-formats is automatically included in FIJI).

6.2. Create a theoretical point-spread function (PSF) using the ImageJ plugin, **Diffraction PSF 3D**.

NOTE: Each imaging channel requires its own PSF as fluorescent protein emission wavelength impacts the PSF.

6.3. Use **Plugins | Macros | Run** to perform batch **Parallel Iterative Deconvolution** for all timepoints using the provided **macro** (**Supplementary File 1**).

NOTE: This macro runs 25 iterations of the Wiener Filter Preconditioned Landweber (WPL) iterative algorithm. Each color channel must be deconvolved separately.

6.4. Merge the color channels, and compile all time points into a Hyperstack (**Image | Hyperstacks | Stacks to Hyperstack**). Correct the 3D drift using **Plugins | Registration | Correct 3D Drift**.

6.5. Return the image to a regular stack (**Image | Hyperstacks | Hyperstack to Stack**), and split the time points (**Image | Stacks | Tools | Stack Splitter**). Use batch processing to create maximum projection for all time points (**Process | Batch | Macro | *run("Z Project...", "projection=[Max Intensity]");***).

6.6. Import the time-lapse image sequence (**File | Import | Image Sequence**). Use conventional ImageJ tools for desired analysis of deconvolved and post-processed two-dimensional (2D) video.

NOTE: Four-dimensionally (3D + time) deconvolved and drift-corrected videos can be viewed as a hyperstack. Omit the previous step to maintain 3D time points.

REPRESENTATIVE RESULTS:

Using the above protocol, a high-resolution 3D video of developing starburst cell dendrites was acquired, deconvolved, and corrected for 3D drift. Z-plane maximum projections were produced to make 2D videos for analysis (**Supplementary Video 1**, **Figure 5A**). 3D deconvolution of each time point increased the resolution of fine filopodia projections (**Figure 5B,C**). Fine filopodia protrusions are a feature of developing retinal dendrites[36] and should be visible during imaging. AAV transfection will produce variability in cell labeling density and fluorescence intensity. Thus, screen the labelled tissue to select cells with high fluorescent signals for imaging and producing high-quality videos. Increasing the laser power to detect dimly labelled cells is not recommended, as it can lead to rapid photobleaching and introduce high noise compared to the signal. Sufficiently bright cells are visible within 5 dpi. By 12 dpi and beyond, prolonged AAV infection periods do not necessarily lead to increased fluorescence of labeled cells (**Figure 5D**).

Excessive fluorescence and neurite crowding from dense cell labelling affects image quality and can hinder single-cell reconstructions. Optimization of the AAV dilution and volume is required to achieve the desired degree of isolated and fluorescently labeled arbors that are separable from the rest of the target cell population. Here, 9.2×10^8–1.8×10^9 viral GCs were injected per eye to target starburst amacrine cells (0.23–0.45 µL of AAV with a 4×10^{12} GC/mL titer). The absence of a fluorescent signal might reflect an inefficient injection technique. While injecting, leakage of the blue AAV solution from the injection site indicates that the virus is not delivered to the retina, or that the injection volume or pressure is too high. Excess injection volume or pressure can cause retinal detachment and/or loss of ocular pressure, damaging the retinal cells and reducing cell-labeling efficiency. Both issues can be resolved with practice and optimization of the injection technique. Other potential reasons for the lack of signal include degradation of the AAVs from improper storage or insufficient *Cre* expression because the *Cre* transgene is not active during the period of AAV transfection.

Once videos are deconvolved, dynamic analyses, such as calculating rates of branch addition, retraction, or stabilization, can be performed. Additionally, conventional static analysis can be performed on each timeframe, including neuron reconstruction and morphometric quantifications such as total branch length, branch angles, branch order, or number of terminal branch points. The result of this protocol is a time series of high-resolution 3D image stacks. Most 3D neurite dynamic videos are manually quantified as a maximum projection using an open-source image visualization software such as ImageJ[37]. Another open-source tool, Vaa3D[38], has been developed specifically for visualization of large volumes. If videos are to be analyzed in 3D, use of a 3D + time visualizer such as Vaa3D is recommended. ImageJ and Vaa3D allow direct access to the pixels or voxels in the image, but often neuron reconstructions are created by converting pixel data into skeletonized tree reconstructions. Automatic or semi-automatic neuron reconstructions for single time points can be performed with open-source[39–41] and proprietary software. To analyze time-lapse reconstructions, each point on the reconstruction must be linked to the previous and the subsequent time points. Aligning complex dendritic morphologies over time, which can be encoded by upwards of 500 data points, remains a

challenging problem. Many tools are available, with different strengths and limitations, and they must be selected to suit the analyses needed for the study.

FIGURE AND TABLE LEGENDS:

Figure 1: Experimental overview. (**A**) This protocol spans 2 days of experiments with a minimum of 4–5-day infection period between experimental days. Intraocular injections are performed on neonatal mice no older than postnatal day 3. Retinas are then dissected, flat-mounted, and live-imaged to capture the desired developmental window. Labelled cells can be imaged any time after the required 4–5 days needed for viral expression, as there are no apparent effects of prolonged AAV expression on dendrite morphology. (**B**) Cre-dependent Brainbow AAV vectors (BBV) are injected into animals expressing Cre. In this study, ChAT-Cre knock-in mice were used to drive Cre recombination in starburst amacrine cells. The two BBVs encode modified eYFP or tagBFP, or mCherry and mTFP, which terminate in a *CAAX* motif that is sequentially farnesylated for membrane localization. Lox sites are depicted with triangles. The vectors express either farnesylated XFPs in a stochastic and combinatorial manner dependent on Cre recombination. The *EF1α* promoter includes regulatory elements from the elongation factor 1α gene. W represents elements from the woodchuck hepatitis virus posttranscriptional regulatory element, and pA indicates the polyadenylation sequence. (**C**) The excitation and emission spectra of mCherry and eYFP, the BBV fluorophores imaged in this study. When live-imaging multiple fluorescent proteins, the detection parameters must be arranged to adequately separate emission spectra into distinct channels. Abbreviations: AAV = adeno-associated virus; BBV = Brainbow AAV; ChAT = choline acetyltransferase; iRES = internal ribosome entry site; eYFP = enhanced yellow fluorescent protein; iTR = inverted terminal repeat; tagBP = Tag-blue fluorescent protein; mCherry = monomeric Cherry; mTFP = teal fluorescent protein; XFP = any fluorescent protein; EF1α= elongation factor 1 alpha.

Figure 2: Neonatal intraocular injections. (**A**) Backfilled micropipette shows the shape of the pipette tip when sealed (top) and after the tip is unsealed (bottom, left). Pico-injection pressure of 6–8 psi and pulse time of 600–800 ms produces a 600 µm diameter droplet (bottom, right). Scale bar = 1 mm. (**B**) Anesthetized P0 pup under 16x magnification. The fused eyelid junction (white) is slit open using a sharp 30 G needle. Scale bar = 2 mm. (**C**) Light pressure applied to the eye exposes the cornea; scale bar = 2 mm. Zoomed section (red) shows the small hole at the cornea-sclera junction (yellow) created with a 30 G needle; scale bar = 0.5 mm. (**D**) Withdrawal of the pipette tip after injection (left). Fast Green dye in the AAV solution appears as blue-grey through the pupil (middle), as compared to the light pupil color before injection (right). Scale bar = 1 mm. (**E**) After 4 days, the eyelid has healed and fused shut (left); scale bar = 2 mm. Upon enucleation, the healed injection site is visible (yellow); scale bar = 1 mm. Note the location of the injection site at the border between the cornea and sclera.

Figure 3: Retinal dissection and flat-mounting onto mixed cellulose ester filter membranes. (**A**) Left, an enucleated eye is stabilized by grasping the optic nerve with Dumont #5 forceps (left). A small hole is created in the center of the cornea using a 30 G needle (center). Micro-dissection scissors are used to cut the cornea into 4 equal flaps (right). Scale bar = 1 mm. (**B**) Dissected retina with the sclera peeled off using two Dumont #5 forceps (left) and with the lens

removed (center). Retina with 4 equal cuts halfway into the retina (right). Scale bar = 1 mm. (**C**) Handling of retina with two fine paintbrushes (size 3/0, left). Retina flipped with retinal ganglion cells side down onto a paintbrush (center) and lifted out of aCSF, making sure the water tension does not tear the retina (right). Scale bar = 2 mm. (**D**) Grey MCE membrane disc placed onto a white filter paper (left). A droplet of aCSF on the MCE disc (right). Scale bar = 1 cm. (**E**) After floating the retinas into the droplet and positioning them, create a water bridge with the white filter paper to wick the aCSF, pulling the retina onto the charged MCE paper (left); scale bar = 1 cm. Zoomed image of the MCE membrane (red) shows 2 retinas mounted with retinal ganglion cells side up (right); scale bar = 2 mm. One retina is outlined in white. Abbreviations: MCE = mixed cellulose ester; aCSF = artificial cerebrospinal fluid.

Figure 4: Live-cell imaging incubation chamber setup. (A) Live-imaging incubation apparatus showing heating, solution, and imaging components. Dual heater includes a heated incubation chamber platform (back circle with blue connector electrodes) and an in-line solution heater. (**B**) Schematic diagram of **4A**. Retinal flat-mount (red) on MCE membrane (grey) is placed in the incubation chamber. The in-line solution heater is connected to a solution pump (not pictured in **4A**). Imaging chamber dimensions allow a good working area for the dipping objective nose. (**C**) 25x view a retinal explant injected with 0.23–0.45 µL of 4×10^{12} GC/mL of AAV dilution; scale bar = 100 µm. Dense labeling of cells often surrounds the optic nerve head (dashed line, bottom right); scale bar = 50 µm. Abbreviations: MCE = mixed cellulose ester; GC = genome copies; mCherry = monomeric Cherry; eYFP = enhanced yellow fluorescent protein.

Figure 5: Representative results after neonatal intraocular injection, time-lapse imaging, and deconvolution. (**A**) Maximum projections of deconvolved time-lapse imaging series (h:min) of P6 starburst amacrine cell 5 days postAAV injection. Fine filopodia dynamics can now be analyzed using conventional ImageJ tools. An area of dendritic refinement (red box) and an area of dendritic outgrowth (green box) are highlighted. (**B, C**) Single P6 starburst amacrine cell labelled with membrane-tagged eYFP 5 days postAAV injection (dpi) shows bright single-cell labelling. Scale bars for upper panels = 50 µm; scale bars for lower panels = 25 µm. Before (**A**) and after (**B**) deconvolution with ImageJ. Insets (red) show deblurring as a result of successful deconvolution. (**D**) P6 starburst amacrine cell 5dpi (left) compared to P12 starburst cell 11 dpi shows similar levels of fluorescent protein expression. Increasing AAV incubation times do not increase fluorescent signal. The fluorescent signals do not decline with longer AAV infection periods. Identical acquisition and postprocessing parameters were applied to both images. Increased branch thickness and varicosities observed at P12 are normal features of maturing starburst cells and not a labelling or imaging artifact. Scale bars = 10 µm. Abbreviations: AAV = adeno-associated virus; eYFP = enhanced yellow fluorescent protein; dpi = days postinfection.

Figure 6: Considerations for Cre line selection and fluorescent protein localization.
(**A–D**) Live P11 retinal ganglion cells imaged at 9 dpi of the BBV injected into Vglut2-iRES-Cre knock-in mice, in which Cre is selectively expressed in the RGC population. (**A**) JAM-B RGC identified by its characteristic asymmetric morphology[24]. (**B–D**) Distinct RGC subtypes that differ in their dendrite stratification patterns. (**E**) Image of live P11 starburst amacrine cell biolistically transfected with cytosolic mCherry and captured with spinning disk confocal at 512

x 512 pixels. The cytosolic XFP leads to high fluorescence signal in the soma relative to the fine dendritic protrusions. Out-of-focus light from the soma causes high background fluorescence when imaging small proximal projections (inset in red box above is shown below). (**F**) Image of live P11 starburst amacrine cell transfected with membrane-targeted eYFP and captured by confocal laser scanning at 1024 x 1024 pixels. Note the fluorescent membrane ring around the soma, the improved signal-to-noise ratio, and quality of the fine projections proximal to the soma that are produced by membrane-targeted fluorescent proteins (inset). Scale bars = 50 µm and for lower panels of **E** and **F** = 5 µm. Abbreviations: iRES = internal ribosome entry site; BBV = Brainbow adeno-associated virus; Vglut2 = vesicular glutamate transporter 2; XFP = any fluorescent protein; eYFP = enhanced yellow fluorescent protein; mCherry = monomeric Cherry; RGC = retinal ganglion cells; JAM-B = junction adhesion molecule B.

Supplementary Video 1: Time-lapse video of P6 developing starburst amacrine dendrites, 5 days postinjection. Video time-step is 2 min. Deconvolution and 3D drift correction were applied using ImageJ. Top yellow boxes highlight areas of outgrowth, and the lower box outlines a region of transient filopodia outgrowth, self-contact, and retraction.

Supplemental File 1: ImageJ macro for batch **Parallel Iterative Deconvolution**. The macro runs 25 iterations of the Wiener Filter Preconditioned Landweber (WPL) iterative algorithm.

DISCUSSION:

This video demonstrates an experimental pipeline that utilizes existing genetic tools to image dendrite dynamics of developing retinal neurons with confocal live-imaging. Also demonstrated are intraocular injections of Cre-dependent AAVs encoding membrane-targeted fluorescent proteins into neonatal mice. Single cells of genetically targeted populations are brightly labelled as early as 4–5 dpi. Retinal flat-mounts were prepared for standard imaging chambers to perform live-cell confocal imaging. This method produces high-resolution time-lapse videos of single cells and their fine projections. Small projections are resolved and quantified using deconvolution and postprocessing algorithms available through open-source software, including ImageJ, Vaa3D, and ShuTu, as well as licensed software available from Imaris and MBF Bioscience. As this pipeline is modular, each protocol section can be altered to fit the objectives of the study. These modular elements are discussed below and include: 1) Cre-line selection, 2) choice of fluorescent protein and viral construct, 3) gene delivery methods, and 4) imaging method.

This technique uses Cre transgenic lines for genetic access to retinal cell subpopulations. Cre must be active postnatally and expressed across the cell population at the time of injection to increase the probability of viral infection and cell labeling. In this report, ChAT-Cre was used to target starburst amacrine cells, and the Vglut2-Cre line was used to target developing RGCs[42,43] **(Figure 6)**. Cre-dependent AAV injection into Vglut2-IRES-Cre knock-in mice labelled a variety of RGCs, including the junction adhesion molecule B cell (**Figure 6A**) and bi-stratified RGCs (**Figure 6B, C**). Alternatively, new designs of AAVs with synthetic promoters that drive cell type-specific expression could eliminate the need for Cre transgenic lines[44]. Another consideration for efficient and bright labeling suitable for live-imaging is the minimum time required for

transfection and expression, which can vary depending on the AAV serotype, tropism, and titer[45]. In these studies, as AAV-mediated labeling requires a minimum of 4–5 dpi for XFP expression, this method is not suitable for accessing early postnatal timepoints. To capture early timepoints (e.g., P0–P4), intraocular injections can be performed in utero in embryonic animals, as done for in utero electroporation[46]. In this group's studies of starburst dendrite development, the initial sparse recombination pattern of ChAT-Cre was exploited to label single starburst amacrine cells at P0–P4 using a mouse transgenic Cre reporter, Rosa-mTmG[27]. Finally, this AAV retinal injection protocol can be used to label adult cell populations, based on the confirmation of the persistence of fluorescent labeling 3 months after injection without deleterious effects on starburst cell morphology[34].

This pipeline also allows for flexibility in viral construct selection. To capture dendrite dynamics, a variety of fluorescent reporter proteins can be used, including proteins that localize to specific subcellular structures, proteins of interest, or report functional changes such as actin dynamics (e.g., LifeAct) and calcium signals (e.g., GCaMP). Any commercially available or cloned AAV vector can be employed, and online tools such as fpbase.org should be referenced for brightness and photostability. Here, Brainbow viral vectors encoding fluorescent proteins with a H-Ras farnesylation *CAAX* motif were used for membrane localization. Early in protocol development, cytosolic localization of XPFs was found to be not ideal for studying fine neurite morphology, with an oversaturation of signals from the soma and poor labeling of fine branches (**Figure 6E**). By comparison, membrane-targeted fluorescent proteins were shown to label and resolve fine dendritic protrusions (**Figure 6E,F**). Another consideration is the size, design, and complexity of the viral construct, which can affect the expression time. For example, AAV-CAG-FLEx-mClover3-CAAX was generated, which expresses one XFP in a Cre-dependent manner. This construct has a simpler design, and results in efficient expression by 4 dpi. Together, the diverse options for Cre lines, AAV designs, and fluorescent protein reporters that are widely available from repositories (e.g., JAX, Addgene, and Viral Vector Cores) render this pipeline adaptable to a variety of studies of cell types and developmental phenomena in the retina.

Although this protocol details intraocular AAV injections, other gene delivery methods are available such as plasmid electroporation[46] and biolistic gene delivery (e.g., Gene Gun)[7]. Electroporation requires applying an electric pulse, and biolistic gene delivery requires ex vivo incubation of retinal explants. AAV labeling is less invasive than both these methods and permits acute preparations of retina explants just prior to imaging. Compared to biolistic gene delivery (**Figure 6E,F**), AAV injections resulted in enhanced tissue viability that was better suited for continuous acquisition needed to tracking neurite dynamics. With proper technique, AAV labeling poses little to no damage to the retina, as judged by the health of the tissue at the time of dissection. Intravitreal injections primarily infect cells within the ganglion cell layer and the inner nuclear layer, such as the RGCs and amacrine cells. Many dozens of starburst amacrine cells are typically labeled, with an increased density of labelled cells around the optic nerve head (**Figure 4C**). However, with all three transfection methods, optic nerve severing is unavoidable to obtain retinal explants and will lead to RGC degeneration. Despite optic nerve severing, studies report viable retinal explants from a variety of vertebrate models for 36 h and up to 6 days postenucleation[5,6,7,47,48].

Lastly, the utility of confocal microscopy to capture dendrite dynamics has been demonstrated. Typically, an imaging session spans 2–4 h, and is concluded before tissue degradation or neurite blebbing is observed. Imaging sessions up to 6 h have been conducted; however, the upper limit has not been systematically tested. Areas might undergo photobleaching due to prolonged imaging, but cells in other fields-of-view in the explant remain viable for live-imaging. This method can also be extended to multiphoton or lightsheet microscopy to image neuronal morphology in deeper layers and larger volumes. Multiphoton imaging has been performed to study neurite dynamics in mouse retina and is better suited for studying cells in deeper retinal lamina (e.g., horizontal or photoreceptor cells)[49]. Recently, live-cell lightsheet microscopy was used to capture retinal angiogenesis[50], offering a new avenue for live-imaging of morphogenesis in whole retina. Live-cell lightsheet microscopy could be used to study neural circuit assembly at larger scales, such as axon-dendrite targeting. Multicolor live-imaging is another application of this pipeline that can be used to investigate cell-cell interactions, such as the influence of neighboring cells on dendrite development or other developmental phenomena such as tiling of retinal cells including RGC subtypes[1], microglia, and astrocytes.

In conclusion, a challenging aspect of developmental studies is gaining access at these critical timepoints. This protocol provides a method to visualize morphogenesis that occurs during a specific temporal window. The pipeline combines existing tools and techniques to genetically target cell populations and express membrane-targeted fluorescent proteins. Acute retinal flat-mount preparations maintain viability and fluorescent signals for live-cell confocal imaging over several hours. Transient and dynamic aspects of dendrite development are captured in 3D videos and are post-processed using open-source software. The ability to capture high-resolution 3D videos is essential in investigating dynamic developmental processes.

ACKNOWLEDGEMENTS:

We thank Madison Gray for giving me a hand when I didn't have any. This research was supported by an NSERC Discovery Grant (RGPIN-2016-06128), a Sloan Fellowship in Neuroscience and a Canada Research Chair Tier 2 (to J.L.L). S. Ing-Esteves was supported by the Vision Science Research Program and NSERC Postgraduate Scholarships-Doctoral.

DISCLOSURES:

The authors do not have anything to disclose.

REFERENCES:

1. Lefebvre, J. L., Sanes, J. R., Kay, J. N. Development of dendritic form and function. *Annual Review of Cell and Developmental Biology* **31**, 741–777 (2015).
2. Graham, H. K., Duan, X. Molecular mechanisms regulating synaptic specificity and retinal circuit formation. *Wiley Interdisciplinary Reviews Developmental biology*. **10** (1), e379 (2021).
3. Godinho, L. et al. Targeting of amacrine cell neurites to appropriate synaptic laminae in the developing zebrafish retina. *Development.* **132** (22), 5069–5079 (2005).
4. Mumm, J. S. et al. In vivo imaging reveals dendritic targeting of laminated afferents by zebrafish retinal ganglion cells. *Neuron.* **52** (4), 609–621 (2006).

5. Wong, W. T., Faulkner-Jones, B. E., Sanes, J. R., Wong, R. O. Rapid dendritic remodeling in the developing retina: dependence on neurotransmission and reciprocal regulation by Rac and Rho. *The Journal of Neuroscience.* **20** (13), 5024–5036 (2000).
6. Wei, W., Elstrott, J., Feller, M. B. Two-photon targeted recording of GFP-expressing neurons for light responses and live-cell imaging in the mouse retina. *Nature Protocols.* **5** (7), 1347–1352 (2010).
7. Morgan, J. L., Wong, R. O. L. Ballistic labeling with fluorescent dyes and indicators. *Current Protocols in Neuroscience.* **43** (1), 2.11.1–2.11.10 (2008).
8. Nickerson, P. E. B. et al. Live imaging and analysis of postnatal mouse retinal development. *BMC Developmental Biology.* **13**, 24 (2013).
9. Morgan, J. L., Dhingra, A., Vardi, N., Wong, R. O. L. Axons and dendrites originate from neuroepithelial-like processes of retinal bipolar cells. *Nature Neuroscience.* **9** (1), 85–92 (2006).
10. Coombs, J. L., Van Der List, D., Chalupa, L. M. Morphological properties of mouse retinal ganglion cells during postnatal development. *The Journal of Comparative Neurology.* **503** (6), 803–814 (2007).
11. Cranfill, P. J. et al. Quantitative assessment of fluorescent proteins. *Nature Methods.* **13** (7), 557–562 (2016).
12. Stacy, R. C., Wong, R. O. L. Developmental relationship between cholinergic amacrine cell processes and ganglion cell dendrites of the mouse retina. *The Journal of Comparative Neurology.* **456** (2), 154–166 (2003).
13. Kay, J. N. et al. Retinal ganglion cells with distinct directional preferences differ in molecular identity, structure, and central projections. *The Journal of Neuroscience.* **31** (21), 7753–7762 (2011).
14. Liu, J., Sanes, J. R. Cellular and molecular analysis of dendritic morphogenesis in a retinal cell type that senses color contrast and ventral motion. *The Journal of Neuroscience.* **37** (50), 12247–12262 (2017).
15. Diao, L., Sun, W., Deng, Q., He, S. Development of the mouse retina: emerging morphological diversity of the ganglion cells. *Journal of Neurobiology.* **61** (2), 236–249 (2004).
16. Coombs, J., van der List, D., Wang, G. Y., Chalupa, L. M. Morphological properties of mouse retinal ganglion cells. *Neuroscience.* **140** (1), 123–136 (2006).
17. Sanes, J. R., Masland, R. H. The types of retinal ganglion cells: current status and implications for neuronal classification. *Annual Review of Neuroscience.* 38, 221–246 (2015).
18. Sümbül, U. et al. A genetic and computational approach to structurally classify neuronal types. *Nature Communications.* **5**, 3512 (2014).
19. Lin, B., Masland, R. H. Populations of wide-field amacrine cells in the mouse retina. *The Journal of Comparative Neurology.* **499** (5), 797–809 (2006).
20. Macneil, M. A., Heussy, J. K., Dacheux, R. F., Raviola, E., Masland, R. H. The shapes and numbers of amacrine cells: Matching of photofilled with Golgi-stained cells in the rabbit retina and comparison with other mammalian species. *Journal of Comparative Neurology.* **413** (2), 305–326 (1999).
21. Ivanova, E., Hwang, G. S., Pan, Z. H. Characterization of transgenic mouse lines expressing Cre recombinase in the retina. *Neuroscience.* **165** (1), 233–243 (2010).

22. Jo, A., Xu, J., Deniz, S., Cherian, S., DeVries, S. H., Zhu, Y. Intersectional strategies for targeting amacrine and ganglion cell types in the mouse retina. *Frontiers in Neural Circuits.* **12**, 66 (2018).
23. Siegert, S. et al. Genetic address book for retinal cell types. *Nature Neuroscience.* **12** (9), 1197–1204 (2009).
24. Kim, I.-J., Zhang, Y., Meister, M., Sanes, J. R. Laminar restriction of retinal ganglion cell dendrites and axons: subtype-specific developmental patterns revealed with transgenic markers. *The Journal of Neuroscience.* **30** (4), 1452–1462 (2010).
25. Peng, Y.-R., Tran, N. M., Krishnaswamy, A., Kostadinov, D., Martersteck, E. M., Sanes, J. R. Satb1 regulates contactin 5 to pattern dendrites of a mammalian retinal ganglion cell. *Neuron.* **95** (4), 869–883.e6 (2017).
26. Duan, X., Krishnaswamy, A., De la Huerta, I., Sanes, J. R. Type II cadherins guide assembly of a direction-selective retinal circuit. *Cell.* **158** (4), 793–807 (2014).
27. Ray, T. A. et al. Formation of retinal direction-selective circuitry initiated by starburst amacrine cell homotypic contact. *eLife.* **7**, e34241 (2018).
28. Krishnaswamy, A., Yamagata, M., Duan, X., Hong, Y. K., Sanes, J. R. Sidekick 2 directs formation of a retinal circuit that detects differential motion. *Nature.* **524** (7566), 466–470 (2015).
29. Caval-Holme, F., Zhang, Y., Feller, M. B. Gap junction coupling shapes the encoding of light in the developing retina. *Current Biology.* **29** (23), 4024–4035.e5 (2019).
30. Lucas, J. A., Schmidt, T. M. Cellular properties of intrinsically photosensitive retinal ganglion cells during postnatal development. *Neural Development.* **14** (1), 8 (2019).
31. Cai, D., Cohen, K. B., Luo, T., Lichtman, J. W., Sanes, J. R. Improved tools for the Brainbow toolbox. *Nature Methods.* **10** (6), 540–547 (2013).
32. Rossi, J. et al. Melanocortin-4 receptors expressed by cholinergic neurons regulate energy balance and glucose homeostasis. *Cell Metabolism.* **13** (2), 195–204 (2011).
33. Lefebvre, J. L., Kostadinov, D., Chen, W. V., Maniatis, T., Sanes, J. R. Protocadherins mediate dendritic self-avoidance in the mammalian nervous system. *Nature.* **488** (7412), 517–521 (2012).
34. Ing-Esteves, S. et al. Combinatorial effects of alpha- and gamma-protocadherins on neuronal survival and dendritic self-avoidance. *The Journal of Neuroscience.* **38** (11), 2713–2729 (2018).
35. Williams, P. R., Morgan, J. L., Kerschensteiner, D., Wong, R. O. L. In vitro imaging of retinal whole mounts. *Cold Spring Harbor Protocols.* **2013** (1), doi:10.1101/pdb.prot072645 (2013).
36. Ramoa, A. S., Campbell, G., Shatz, C. J. Transient morphological features of identified ganglion cells in living fetal and neonatal retina. *Science.* **237** (4814), 522–525 (1987).
37. Schindelin, J. et al. Fiji: an open-source platform for biological-image analysis. *Nature Methods*. **9**, 676-682 (2012).
38. Peng, H., Ruan, Z., Long, F., Simpson, J. H., Myers, E. W. V3D enables real-time 3D visualization and quantitative analysis of large-scale biological image data sets. *Nature Biotechnology.* **28** (4), 348–353 (2010).

39. Cuntz, H., Forstner, F., Borst, A., Häusser, M. One rule to grow them all: a general theory of neuronal branching and its practical application. *PLoS Computational Biology.* **6** (8), e1000877 (2010).
40. Xiao, H., Peng, H. APP2: automatic tracing of 3D neuron morphology based on hierarchical pruning of a gray-weighted image distance-tree. *Bioinformatics.* **29** (11), 1448–1454 (2013).
41. Nanda, S. et al. Design and implementation of multi-signal and time-varying neural reconstructions. *Scientific data.* **5**, 170207 (2018).
42. Sherry, D. M., Wang, M. M., Bates, J., Frishman, L. J. Expression of vesicular glutamate transporter 1 in the mouse retina reveals temporal ordering in development of rod vs. cone and ON vs. OFF circuits. *The Journal of Comparative Neurology.* **465** (4), 480–498 (2003).
43. Johnson, J. et al. Vesicular neurotransmitter transporter expression in developing postnatal rodent retina: GABA and glycine precede glutamate. *The Journal of Neuroscience.* **23** (2), 518–529 (2003).
44. Jüttner, J. et al. Targeting neuronal and glial cell types with synthetic promoter AAVs in mice, non-human primates and humans. *Nature Neuroscience.* **22** (8), 1345–1356 (2019).
45. Zincarelli, C., Soltys, S., Rengo, G., Rabinowitz, J. E. Analysis of AAV serotypes 1-9 mediated gene expression and tropism in mice after systemic injection. *Molecular Therapy.* **16** (6), 1073–1080 (2008).
46. Petros, T. J., Rebsam, A., Mason, C. A. In utero and ex vivo electroporation for gene expression in mouse retinal ganglion cells. *Journal of Visualized Experiments: JoVE.* (31), 1333 (2009).
47. Lye, M. H., Jakobs, T. C., Masland, R. H., Koizumi, A. Organotypic culture of adult rabbit retina. *Journal of Visualized Experiments: JoVE.* (3), 190 (2007).
48. Pignatelli, V., Strettoi, E. Bipolar cells of the mouse retina: a gene gun, morphological study. *The Journal of Comparative Neurology.* **476** (3), 254–266 (2004).
49. Huckfeldt, R. M. et al. Transient neurites of retinal horizontal cells exhibit columnar tiling via homotypic interactions. *Nature Neuroscience.* 12 (1), 35–43 (2009).
50. Prahst, C. et al. Mouse retinal cell behaviour in space and time using light sheet fluorescence microscopy. *eLife.* **9**, e49779 (2020).

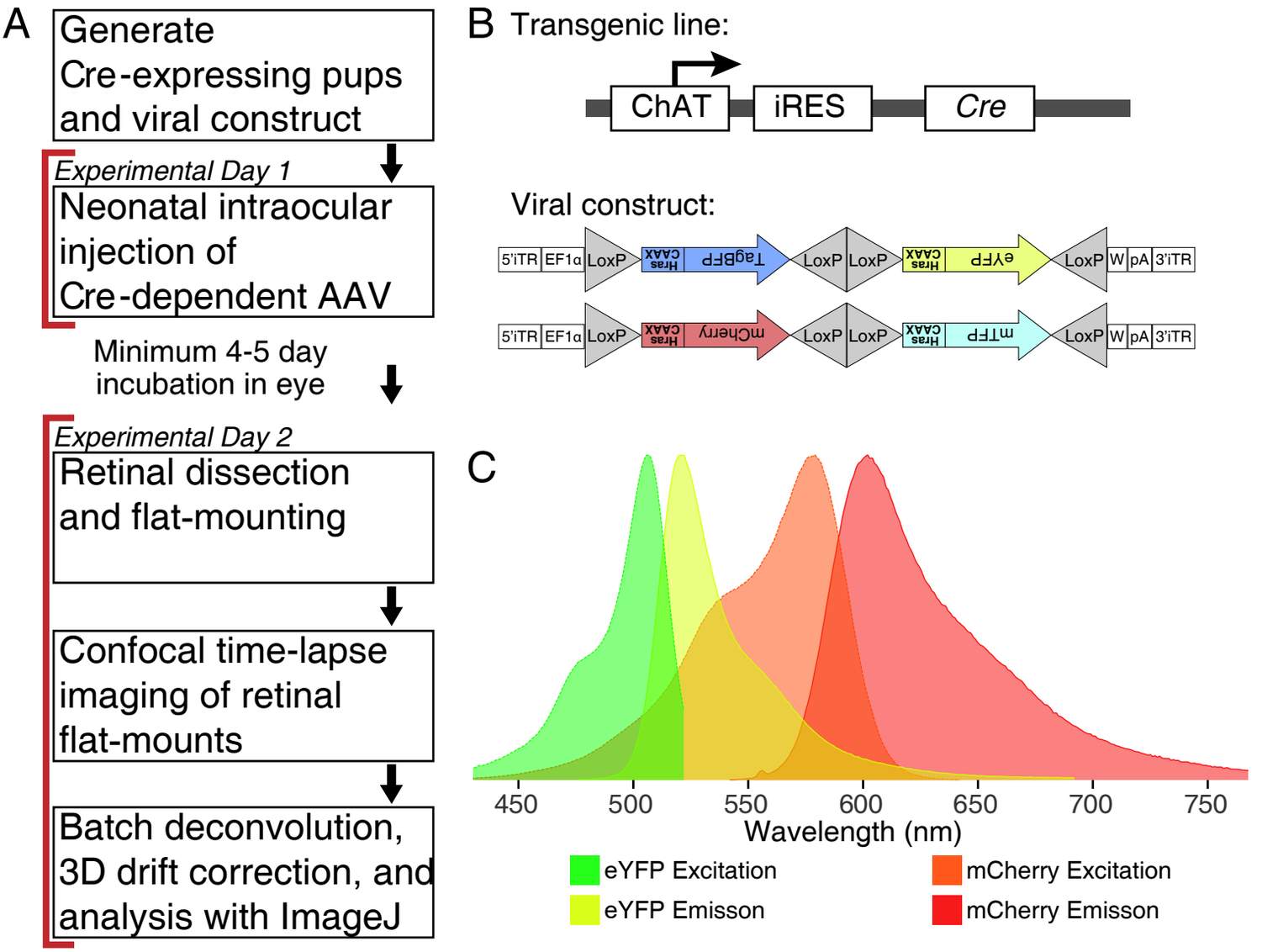

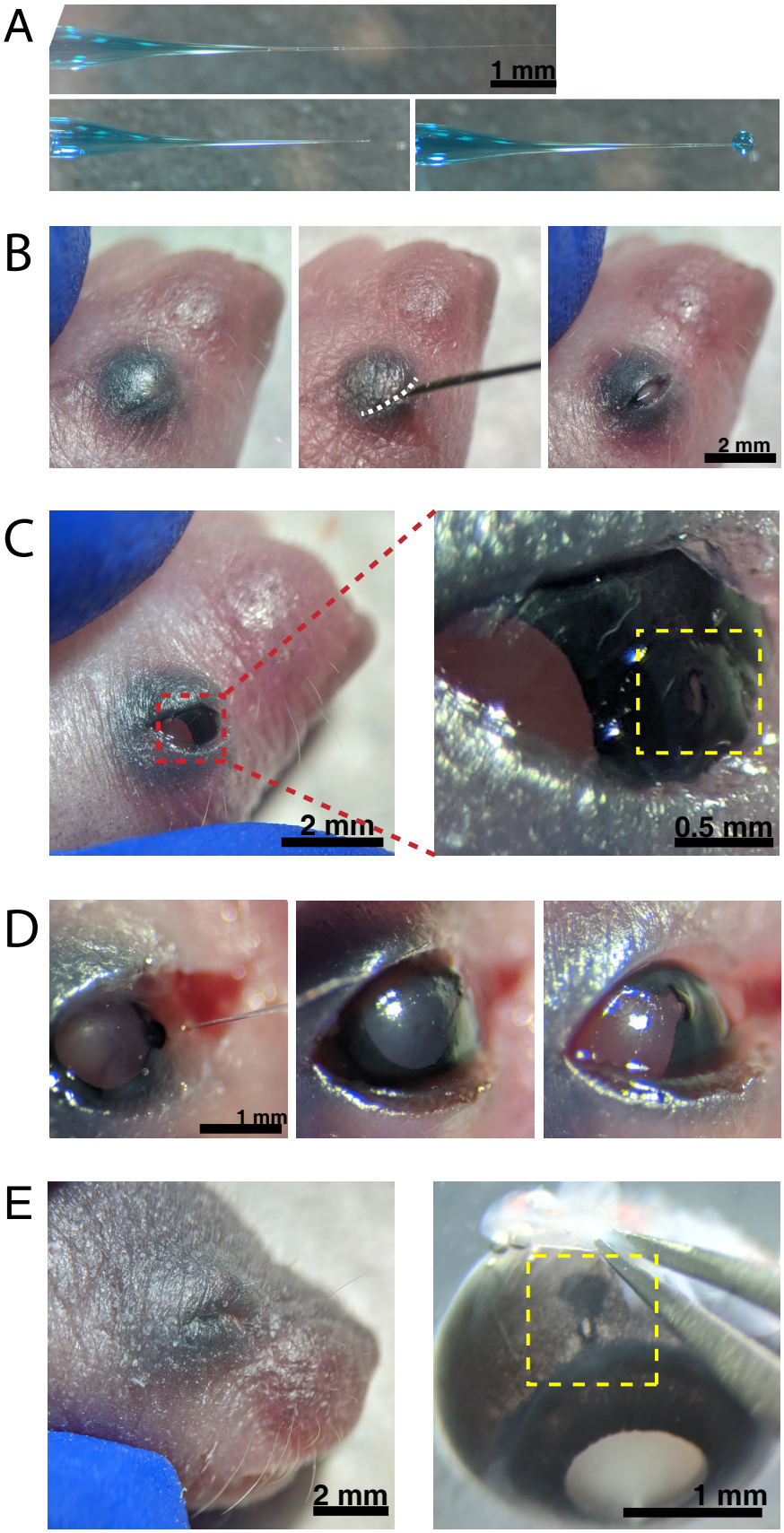

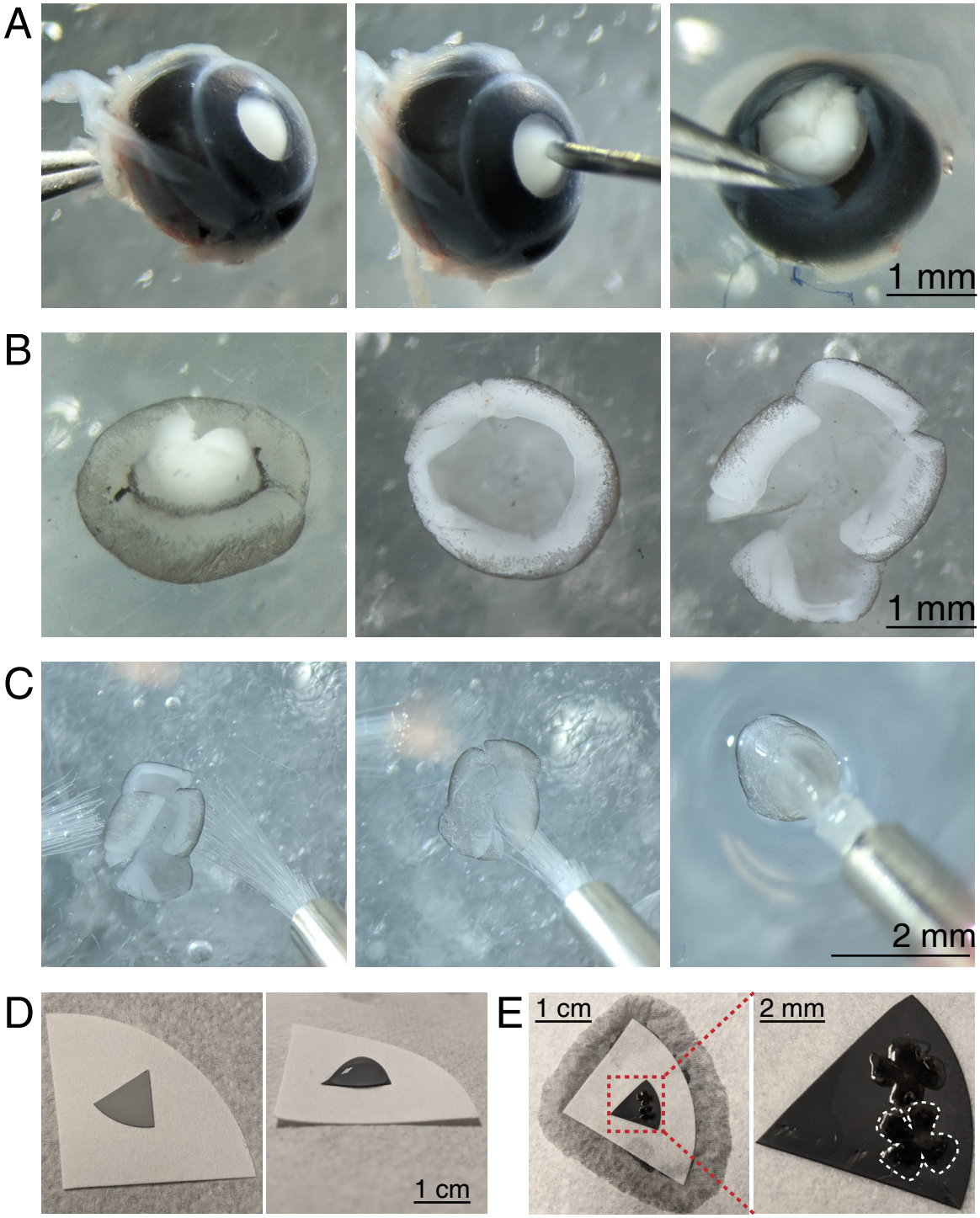

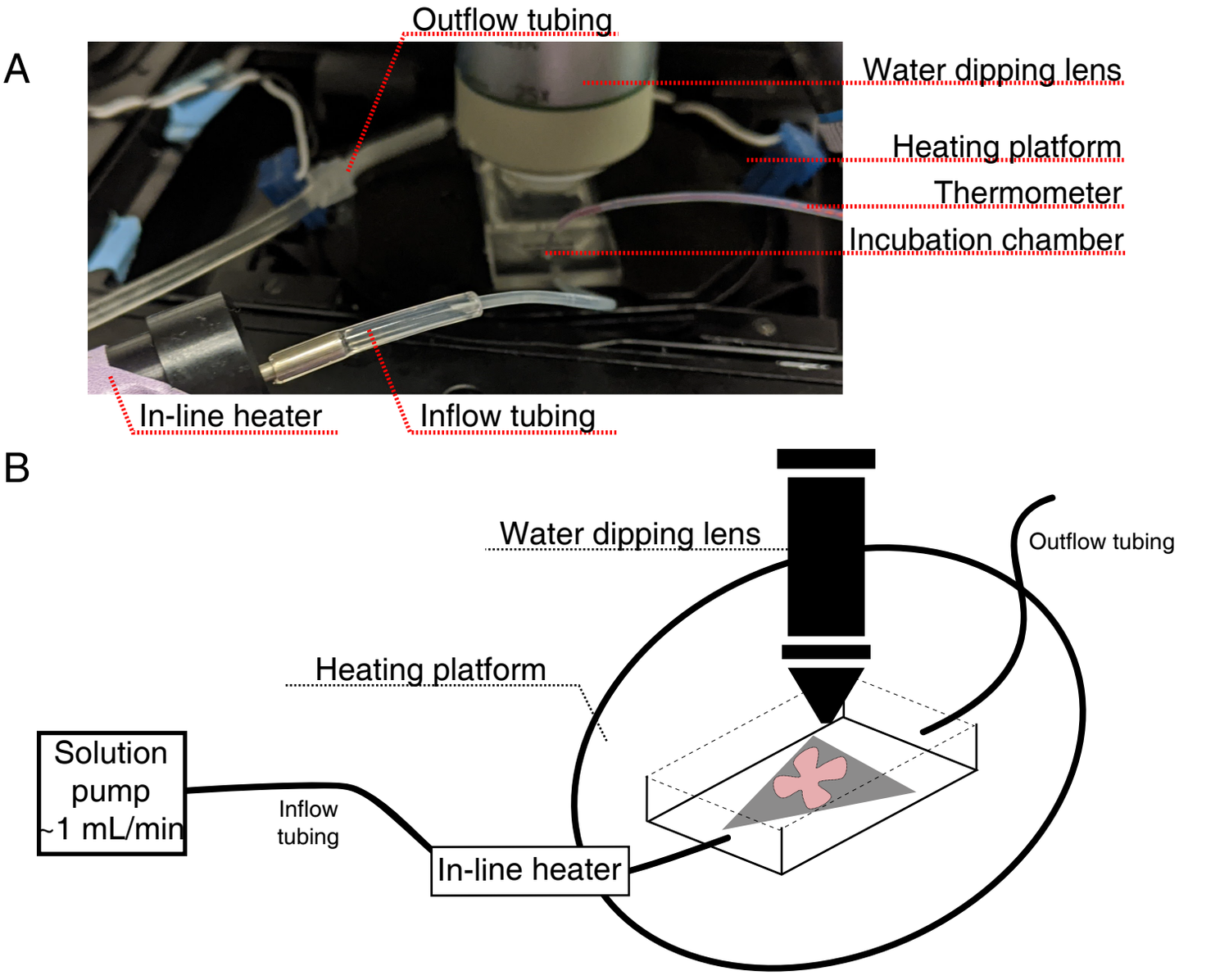

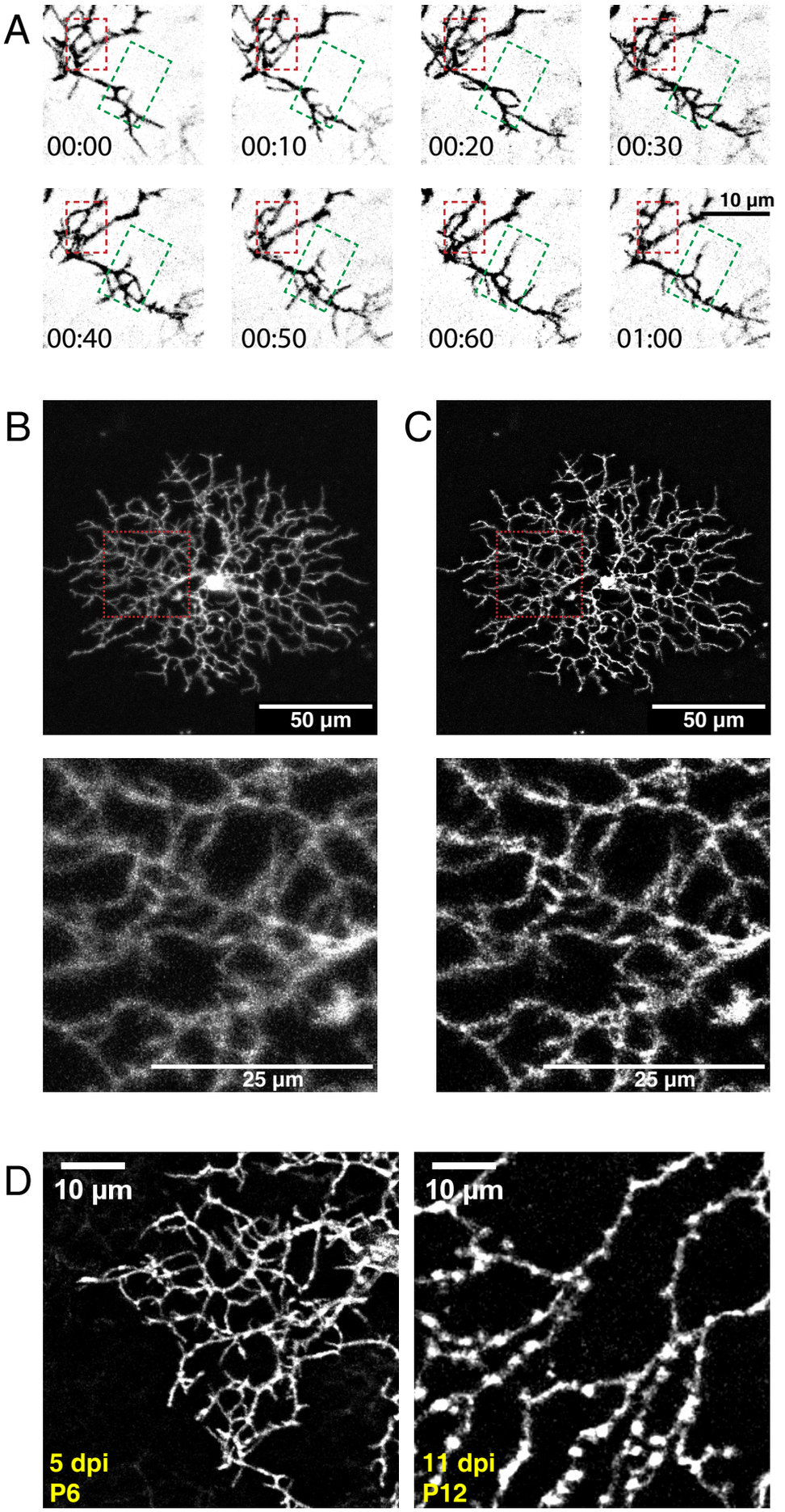

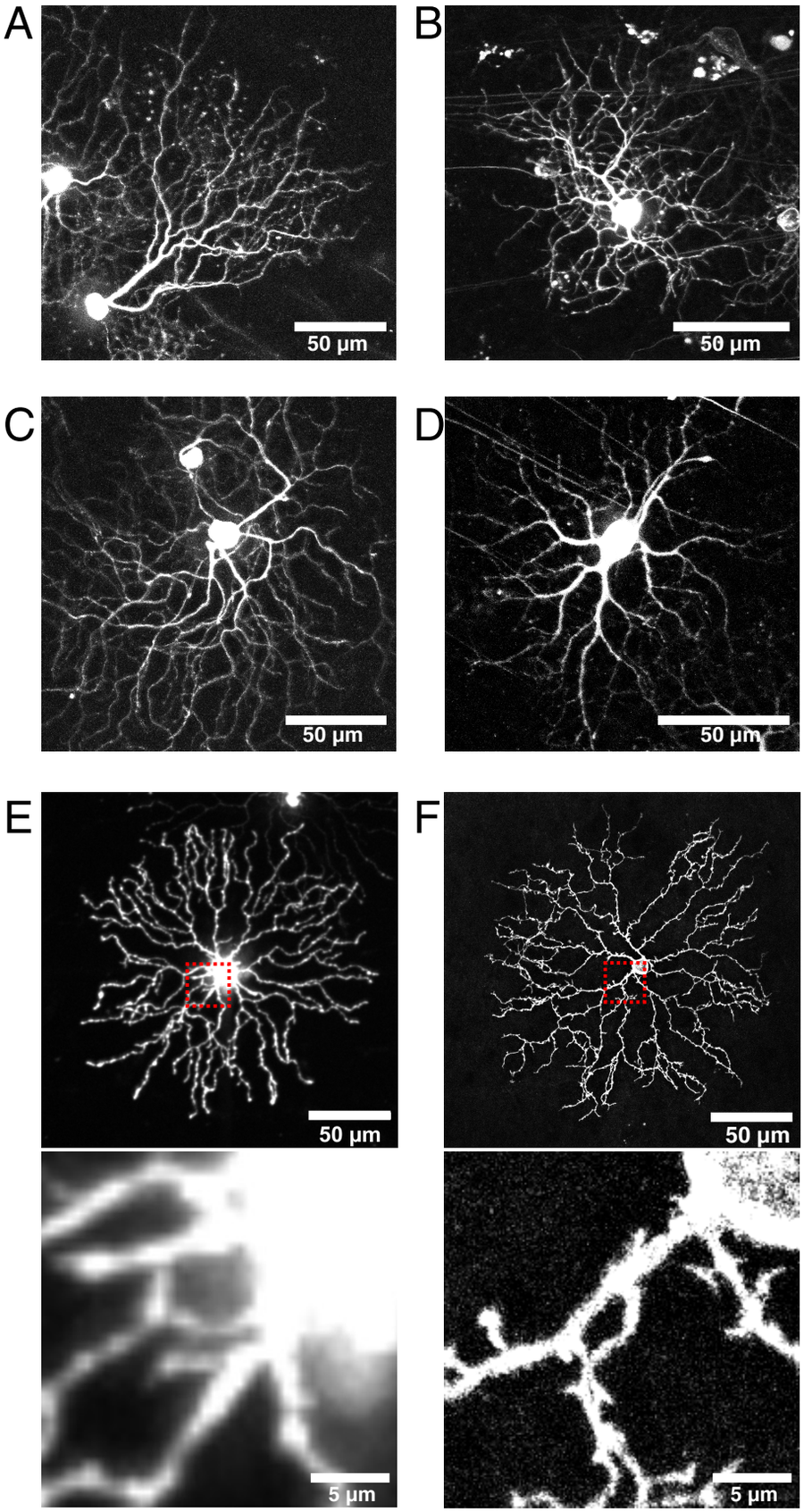

Name of Material/Equipment

Dissection tools

Cellulose filter paper
Dumont #5 fine forceps
Dumont forceps
Fine Scissors
Mixed cellulose ester membrane (MCE) filter papers, hydrophilic, 0.45 µm pore size
Petri Dish, 50 × 15 mm
Polyethylene disposable transfer pipette
Round tip paint brush, size 3/0
Surgical Scissors
Vannas Spring Scissors - 2.5 mm Cutting Edge

Live-imaging incubation system

Chamber polyethylene tubing, PE-160 10'
Dual channel heater controller, Model TC-344C
HC FLUOTAR L 25x/0.95 W VISIR dipping objective
Heater controller cable
Large bath incubation chamber with slice support
MPII Mini-Peristaltic Pump
PM-6D Magnetic Heated Platform (incubation chamber heater)
Pump Head Tubing Pieces For MPII Mini-Peristaltic Pump
Sample anchor (Harps)
Sloflo In-line Solution Heater

Neonatal Injections

10 µL Microliter Syringe Series 700, Removable Needle
30 G Hypodermic Needles (0.5 inch)
4 inch thinwall glass capillary, no filament (1.0 mm outer diameter/0.75 mm)
Ethanol 99.8% (to dilute to 70% with double-distilled water [ddH_2O])
AAV9.hEF1a.lox.TagBFP. lox.eYFP.lox.WPRE.hGH-InvBYF
AAV9.hEF1a.lox.mCherry.lox.mTFP1.lox.WPRE.hGH-InvCheTF
ChAT-IRES-Cre knock-in transgenic mouse line
Fast Green FCF Dye content ≥85 %
Flaming/Brown Micropipette Puller, model P-97
Green tattoo paste
Phosphate-Buffered Saline, pH 7.4, liquid, sterile-filtered, suitable for cell culture
Pneumatic PicoPump

Oxygenated artifiial cerebrospinal fluid (aCSF) Reagents

Calcium chloride dihydrate ($CaCl_2 \cdot 2H_2O$)
Carbogen (5% CO_2, 95% O_2)
D-(+)-Glucose
HEPES, Free Acid
Hydrochloric acid solution, 1 N
Magnesium chloride hexahydrate ($MgCl_2 \cdot 6H_2O$)
pH-Test strips (6.0-7.7)
Potassium chloride (KCl)
Sodium chloride (NaCl)
Sodium phosphate monobasic (NaH_2PO_4)

Software

ImageJ

Company	Catalog Number	Comments/Description
Whatman	1001-070	
FST	11252-20	Two Dumont #5 forceps are required for retina
VWR	82027-426	
FST	14058-09	
Millipore	HABG01 300	
VWR	470313-352	
VWR	470225-034	
Conventional art supply store		Two size 3/0 paint brushes (or smaller) are required for retinal flat-mounting
FST	14007-14	
FST	15000-08	

Company	Catalog Number	Comments/Description
Warner Instruments	64-0755	
Warner Instruments	64-2401	
Leica	15506374	
Warner Instruments	CC-28	
Warner Instruments	RC-27L	
Harvard Apparatus	70-2027	
Warner Instruments	PM-6D	
Harvard Apparatus	55-4148	
Warner Instruments	64-0260	Sample anchor must be compatible with incubation chamber
Warner Instruments	SF-28	

Company	Catalog Number	Comments/Description
Hamilton Company	80314	
BD PrecisionGlide	305106	
WPI World Precision Instruments	TW100-4	
Sigma-Aldrich	V001229	
Penn Vector Core	AV-9-PV2453	Addgene Plasmid #45185
Penn Vector Core	AV-9-PV2454	Addgene Plasmid #45186
The Jackson Laboratory	6410	
Sigma-Aldrich	F7252-25G	
Sutter Instrument Co.	P-97	
Ketchum MFG Co	329A	
Sigma-Aldrich	806552	
WPI World Precision Instruments	PV-820	

Company	Catalog Number	Comments/Description

Sigma-Aldrich	C7902	
AirGas	X02OX95C2003102	Supplier may vary depending on region
Sigma-Aldrich	G7021	
Bio Basic	HB0264	
Sigma-Aldrich	H9892	
Sigma-Aldrich	M2670	
VWR	BDH35317.604	
Sigma-Aldrich	P9541	
Bio Basic	DB0483	
Sigma-Aldrich	RDD007	

Company	**Catalog Number**	**Comments/Description**
National Institutes of Health (NIH)	Open source	

al micro-dissection

Dear Dr. Iyer

We thank you for handling our submission entitled “Time-lapsed imaging of neuronal arborization using sparse AAV labeling of genetically targeted cell populations in retina”. We are submitting the revised manuscript with modified text in red font, including new/revised figures and figure legends.

We have addressed reviewer and editorial comments in full. We provide a point-by-point response to the reviewers suggestions, in red font. We specify the changes made to the manuscript and provide the line number in the document to highlight the modified text in the manuscript. We thank the reviewers for their thoughtful comments and suggestions, and we hope that you will find that our revisions adequately address these comments.

Editorial comments:

Changes to be made by the Author(s):

All the formatting changes listed below (1-12) have been made.

1. Please take this opportunity to thoroughly proofread the manuscript to ensure that there are no spelling or grammar issues.
2. Please define all abbreviations before use. E.g. Line 299-300: PFA, IHS.
3. Include a single space between the quantity and its unit E.g.: 1 cm.
4. Abbreviate liters to L to avoid confusion. E.g.: 10 mL, 8 µL.
5. Use the standard symbol for units. E.g. Line 167: “…-80 oC..” instead of “..-80’C..”, Line 179: “4 oC” instead of “4’C” , Line 291-292: “..µm..” instead of “..um..”
6. Line 170: Please specify the appropriate units for the settings.

Per reviewer #1’s suggestion, we removed puller settings from line 170 because settings vary depending on machine and filament, and will not reproduce final tip specifications.

7. Please do not highlight steps involving euthanasia for filming.
8. Line 252: How is the MCE paper prepared?

This is now included in 4.1 (lines 269-274).

9. Please adjust the numbering of the Protocol to follow the JoVE Instructions for Authors. For example, 1 should be followed by 1.1 and then 1.1.1 and 1.1.2 if necessary.
10. For in-text formatting, corresponding reference numbers should appear as numbered superscripts after the appropriate statement(s). E.g. Line 218
11. Please do not use “&” in the references. Ensure that the references appear as the following: [Lastname, F.I., LastName, F.I., LastName, F.I. Article Title. Source. Volume (Issue), FirstPage – LastPage (YEAR).] For more than 6 authors, list only the first author then et al.
12. Please sort the Materials Table alphabetically by the name of the material.

Table of materials is categorized based on sections of the protocol, which is sequential when conducting the experiment. We maintained the categories in the table, but organized the materials alphabetically within the categories.

Response to Reviewers' comments:

We thank the reviewers for the thoughtful comments and specific suggestions. We have addressed these concerns and revised the manuscript accordingly. As a result of these changes, you will see that we have clarified the protocol and significantly improved the quality of the manuscript.

Reviewer #1:

Manuscript Summary:

The authors described the detailed methods for live imaging of retinal cells during retinal development. The manuscript contains the methodology for ocular injection of AAV vectors at P0, the organotypic culture of the developing retina, and image processing of the data using ImageJ. After the reviewing, I have several comments on the manuscript.

Minor Concerns:

1) Although the authors cited the paper using the Brainbow virus (line 132-134), the vector map of the Brainbow would help understand the strategy of the labeling for the readers. The authors may add the description of the CAAX sequence (line 339-341) in the map.

We thank the reviewer for these suggestions. In Figures 1B and 1C, we added schematics of the Brainbow AAV vectors and the excitation/emission spectra of the fluorescent proteins (XFPs) imaged in this study (mCherry and eYFP). For each BBV XFP, we added the HRas-CAAX to denote the C-terminal farnesylation domain for membrane localization. We describe the components of the AAV vector in the Figure legend.

2) In Figure 5, the low magnification image(s) may be required to see the density of labeled starburst amacrine cells by injection of a certain concentration of AAV. Since the Brainbow virus was used, the multi-color image would be preferred.

A low magnification image was added to Figure 4C, and the field of view depicts multiple starburst cells labelled with mCherry or eYFP. Both the volume injected and final titer are reported in the figure caption (lines 214-216 and 386-388).

Reviewer #2:

Manuscript Summary:

This paper describes a very useful and powerful technique which enables monitoring neuronal structure and dynamics during development. Although transfecting retina with AVV in new-born pups appears quite challenging, the authors describe their approach in detail and step by step, so this publication will greatly help the others to reproduce their method. The images presented in the Results section are very impressive.

Minor Concerns:
Method:
1.5.Prepare borosilicate glass micropipettes with fine tips using a micropipette puller 170 (micropipette puller settings: heat 457, pull 60, velocity 100, time 10).
Please provide the required dimensions of the pipette, and state that the tip should be sealed (as evident from 2.6). Adding a photo of the pipette would also help. The puller settings depend on the filament, and different filaments may require different settings. Therefore, an experimenter will need to know how the final pipette should look.
We thank the reviewer for these important points. To Figure 2A, we added images of the sealed and unsealed pulled pipette tip, with scale bar to clarify final tip dimensions. We do not have the means to measure the diameter of the final pipette tip. Instead, we state the diameter of a typical droplet that we measured with a micrometer. Text was modified in the protocol 1.5, 266 and Figure 2A legend, lines 470-472.

5.7. Acquire images maintaining a laser power below 4% to limit photobleaching. All the lasers differ, and even lasers of the same brand can have variable power. So, 4% power is not very informative here. Laser Intensity will also depend on the brightness of the fluorophore.
We thank the reviewer for this point, as the acquisition will vary with the laser, detectors, and fluorophore brightness. We revised the text in 5.7 that suggests a method using a look-up-table to visualize the pixel intensity and adjusting the laser power to acquire the image with a range of pixel intensity values and minimize oversaturated pixels (lines 320-325).

"To adjust the laser power to an optimal setting, use a look-up-table that identifies both oversaturated and undersaturated pixels. While scanning, adjust laser power such that no pixels are oversaturated (i.e. at an intensity of 255 or above). Reduced laser power is recommended as deconvolution algorithms work optimally when pixels are distributed over the full dynamic range. Pixel intensity should not exceed 254; we determined empirically from our analyses of neurites that pixel values below 170 are ideal for deconvolution."

Results
The video and figure 5 need labels (possibly arrows) pointing to the growing filopodia
Two boxed regions have been added to Figure 5A to show an area of dendritic refinement (red box) and an area of dendritic outgrowth (green box). Yellow boxed regions were added to the Supplementary Video to highlight regions of outgrowth, and filopodia self-contacts and retractions. Lines 504-505 and 477-478.

Lines 332-336 and line 352, Figure 4 - The author must be referring to figure 5, not figure 4
Thank you for noting the error. We corrected the figure numbers in the text.

Discussion:

Do the authors know for how many days FP would be expressed after the transfection? Fig. 1 shows that the pups should be older than P4-5 day. But is there a maximal age? It would be helpful to discuss this.
AAV expression of FPs can last several weeks and, typically, without altering neuronal morphology. Figure 5D shows signal at 11 days post injection. We expanded this point clarified in Figure 5 caption (lines 483-485) and in the discussion (lines 541-543).

In the discussion, line 541- :
"Finally, this AAV retinal injection protocol can be used to label adult cell populations, as we have confirmed the persistence of fluorescent labeling 3 months after injection without deleterious effects on starburst cell morphology [34]".

Reviewer #3:
Manuscript Summary:
In the present manuscript by Ing-Esteves & Lefebvre, the authors describe a method to analyze dendrite morphology in retinal explants by time-lapsed confocal microscopy. The authors propose to use neonatal Cre mouse lines and recombinant adeno-associated viral vectors (AAVs) to sparsely label, with fluorescent proteins, specific retinal populations during development. Then, organotypic culture of retinal flatmounts could be used to image sub-types of amacrine e retinal ganglion cells dendrites during 2-5 hours using confocal microscopy. They also describe a protocol for image processing, including dendrite deconvolution, 3D drift correction and quantifications. As a representative experiment, they used the ChAT-IRES-Cre knock-in mice to target the cholinergic starburst amacrine cells. Then, they injected the AAV9.hEF1a.lox.TagBFP.lox.eYFP.lox.WPRE.hGH-InvBYF viral vector, expressing farnesylated eYFP and tagBFP, to label amacrine cell membrane. They could nicely show the dendritic arborization of P6 starburst amacrine cell.
The authors address relevant and important methods to better understand dendrite morphogenesis. The manuscript is written in a clear and well-structured way. However, there are some points that remains unclear or could be improved and should be addressed in a revised version.

Major Concerns:
- The authors used ChAT-IRES-Cre knock-in mice and AAV9.hEF1a.lox.TagBFP.lox.eYFP.lox.WPRE.hGH-InvBYF to express farnesylated eYFP and tagBFP in cholinergic starburst amacrine cells. A map of the constructs, scheme of the recombination and the spectra of both fluorescent proteins would facilitate the visualization.
We thank the reviewer for the suggestions. We have these figures as Figure 1B, and 1C.

- The authors describe the AAV dilution and the volume per eye, however this is not very clear. 1.25x10e12 gc/mL is the final titer of before dilution? The final volume injected in each eye is 0.25µL? The total time to inject this volume was 600-800ms?
In step 2.2 (lines 183-185), we state the viral titre before and after dilution for preparation. In step 2.9, we state the size of the droplet and total volume per injected into each eye. The volume of one pico-injection pulse is also now visualized in Figure 2A (bottom, right). The total viral titers injected is stated in the representative results, as this is specific to our AAV and cell of interest:
Line 388:
"Here, 9.2x10e8 – 1.8x10e9 viral genome copies were injected per eye to target starburst amacrine cells (0.23-0.45 µl of AAV with a 4×10e12 GC/mL titer)."

- If the broken glass micropipette tip and it inserted in the eye could be shown, would facilitate the visualization of this step. Also show the eye after the injection showing Fast Green dye.
Figure 2A now shows the micropipette tip, and Figure 2D shows the tip being removed from the eye after injection and the comparison of pupil colour before and after injection of virus solution containing the Fast Green dye.

- Lines 294-297: What influences the time of imaging (2-6h)? Is there any anti-bleaching agent that could be added to the chamber? Is there any parameter that could be changed to increase the imaging time?
For the purpose of our experiments, we optimized imaging with more frequent intervals for 2-4 hours, with imaging sessions up to 6 hours. We image nearly continuously at 2 minutes intervals, with each scan taking 1.5 to 1.75 minutes. Longer intervals between timepoints with similar scan speeds (1.5 to 1.75 minutes) allows recovery time between scans and may be optimal for imaging sessions beyond 6 hours. We have not systematically tested imaging longer than 6 hours. The rationale and limits of these imaging times is clarified in the protocol (lines 328-332) and discussion (lines 582-587).

Lines 328- :
"The area of prolonged imaging often photobleaches, but other explant sections remain viable. Multiple regions in a flat-mount can be imaged, each for 2-4 hours, with total incubation time of 6 hours. Imaging sessions beyond 6 hours have not been systematically tested. Neurite degradation and blebbing are sign that the explant viability is declining".

Lines 582:
"Lastly, we demonstrate the utility of confocal microscopy to capture dendrite dynamics. Typically, an imaging session spans 2-4 hours and is concluded before tissue degradation or neurite blebbing is observed. Imaging sessions up to 6 hours have been conducted but the upper limit has not been systematically tested. Areas might undergo photobleaching as a result of prolonged imaging, but cells in other field-of-views in the explant remain viable for live-imaging."

- In lines 287/288, would be nice to have here a low magnification image showing the sparse cells.
This image has been added as Figure 4C.

- Figure 6 should be better described in the Representative Results and Protocol sections. The method used to express mCherry, including the plasmid and transfection, should be described in more details. The image in Figure 6A went through all image processing as the image in Figure 6B?
Description of Figure 6 (now Figure 6E-F) is now explained in the discussion.
The discrepancy is the image acquisition and processing is stated in the figure caption (lines 492-500). Another difference in quality is that the image in Figure 6E was captured at 512x512 pixels, and the image in 6F at 1024x1024 pixels.

The comparison of cytosolic vs membrane targeted proteins is discussed in lines 553-556.

Elaboration and comparison of the transfection protocol is discussed in lines 564-569.

Lines 553 - :
"Here we used the Brainbow viral vectors encoding fluorescent proteins with a H-Ras farnesylation CAAX motif for membrane localization. Early in our protocol development, we found that cytosolic localization of XPFs is not ideal for studying fine neurite morphology, with an oversaturation of signals from the soma and poor labeling of fine branches (Figure 6E)."

Line 566 - :
"The protocol details intra-ocular AAV injections, but other gene delivery methods are available such as plasmid electroporation 45 and biolistic gene delivery (e.g. Gene Gun)7. Electroporation requires applying an electric pulse, and biolistic gene delivery requires ex vivo incubation of retinal explants. AAV labeling is less invasive than both these methods and permits acute preparations of retina explants just prior to imaging. We found that AAV injections compared to biolistic gene delivery (Figure 6E, F) resulted in enhanced tissue viability that was better suited for continuous acquisition needed to tracking neurite dynamics."

- Does axotomy of RGCs, induced by retina dissection, result in changes in RGC and/or amacrine neurite morphogenesis? It is important to address this question.
This is addressed in the discussion (lines 574-577). Retinal explant preparations require the axotomy of RGCs. We cannot directly test the effects of RGC axotomy on RGC or amacrine morphogenesis but established protocols routinely perform electrophysiological and morphological studies of RGCs and amacrine cells in retinal explants. See references 5, 6, 7, 46 and 47.

Line 574 - :
However, with all three transfection methods optic nerve severing is unavoidable to obtain retinal explants and will lead to RGC degeneration. Despite optic nerve severing,

studies report viable retinal explants from a variety of vertebrate models for 36 hours, and up to 6 days post enucleation [5,6,7,46,47].

- The authors did not show exemplary results of RGCs dendrites. Is there any parameter that has to be changed to image these cells?
Figure 6A, B, C, and D now shows BBV labelling of P11 retinal ganglion cells targeted with Vglut2-IRES-Cre. See lines 525-531 for discussion of cre selection.

- The authors did not provide any exemplary quantification. Is there any quantification that can be performed using the images in Figures 5 and 6?
This protocol was developed for an ongoing study. Descriptions of our quantifications are not yet published and will be reported in an upcoming paper. Quantifications are specific to the research question. As an alternative, we elaborate in the representative results the several analysis softwares that are available for morphometric analyses and their benefits. Since these quantification methods have been reported elsewhere, we did not view this as a novel, methodological aspect of this demonstration. Lines 403-415.

-Highlight the critical steps and provide a troubleshooting list/table is also important for replication of this method.
We thank you for the suggestion. For key steps of the protocol, we provide several notes ("**Note:** ...") to point out potential areas for troubleshooting.

The main critical step that produces the most common negative result (no fluorescence signal) is outlined in the representative results (lines 390-397)

"The absence of a fluorescent signal might reflect an inefficient injection technique. While injecting, leakage of the blue AAV solution from the injection site indicates that the virus is not delivered to the retina, or that the injection volume or pressure is too high. Excess injection volume or pressure can cause retinal detachment and/or loss of ocular pressure, damaging retinal cells and reducing cell labeling efficiency. Both issues can be resolved with practice and optimization of the injection technique. Other potential reasons for the lack of signal include degradation of the AAVs from improper storage, or insufficient Cre expression because the Cre transgene is not active during the period of AAV transfection."

Minor Concerns:
- The manuscript lacks examples of different constructs that could be used in this method to label other retinal cell subtypes.
In the discussion, we elaborated on other examples of construct designs and commercially available AAVs, including that that express other XFPs and functional reporters, such as for measuring actin dynamics (ie. LifeAct) and intracellular calcium concentrations (ie. Gcamps). In our own work, we generated AAV (pAAV-CAG-FLEx-mClover3-CAAX), described in lines 556-558. See lines 545-561, and below.

As an alternative to Cre, we also mention and cite AAVs that contain specific promoters that drive vector expression selectively in retinal subpopulations (lines 531-532, reference 43).

Lines 545 - :
“This pipeline also allows for flexibility in viral construct selection. To capture dendrite dynamics a variety of fluorescent reporter proteins can be used, including proteins that localize to specific subcellular structures, proteins of interest, or report functional changes such as actin dynamics (e.g. LifeAct) and calcium signals (e.g.Gcamp). Any commercially available or cloned AAV vector can be employed and online tools such as fpbase.org should be referenced for brightness and photostability. Here we used the Brainbow viral vectors encoding fluorescent proteins with a H-Ras farnesylation CAAX motif for membrane localization.”

- Line 260: Figure 3C or Figure 3D?
This is now corrected.

- Lines 334/336/352: Figure 4… should be changed to Figure 5...
This is now corrected.

- Line 408: here should be: Before (B) and after (C) deconvolution with ImageJ.
This is now corrected.

- Figure 5D: in the right image (P12) the neurites look thicker. Is that true or the magnification is different?
This is correct. It is a result of neurite maturation and synapse formation. The magnification of the images are the same. This has been clarified in the figure caption lines 481-486). The purpose of the figure is to show fluorescent signals do not increase with prolonged incubation time.

```
input = getDirectory("Choose the directory where the TIFF files are");
psf = File.openDialog("Select where the PSF file is stored");

output = input + "deconvolved_25it/";

File.makeDirectory(output)

setBatchMode(true);
list = getFileList(input);
for (i = 0; i < list.length; i++)
        if (endsWith(list[i],'.tif'))
           decon(input, output, list[i], psf);
setBatchMode(false);

function decon(input,output,filename,pathToPsf) {
      //------------------------------------------------------------------
------------------------------------------------------------------------
------------------------------------------------------------------------
------------------------------------------------------------------------
------------------------
      // WPL
      //------------------------------------------------------------------
------------------------------------------------------------------------
------------------------------------------------------------------------
------------------------------------------------------------------------
------------------------
      pathToBlurredImage = input + filename;
      pathToDeblurredImage = output + filename;
      boundary = "REFLEXIVE"; //available options: REFLEXIVE, PERIODIC,
ZERO
      resizing = "AUTO"; // available options: AUTO, MINIMAL,
NEXT_POWER_OF_TWO
      output = "SAME_AS_SOURCE"; // available options: SAME_AS_SOURCE,
BYTE, SHORT, FLOAT
      precision = "SINGLE"; //available options: SINGLE, DOUBLE
      threshold = "-1"; //if -1, then disabled
      maxIters = "25";
      nOfThreads = "8";
      showIter = "true";
      gamma = "0";
      filterXY = "1.0";
      filterZ = "1.0";
      normalize = "false";
      logMean = "false";
      antiRing = "true";
      changeThreshPercent = "0.01";
      db = "false";
      detectDivergence = "true";
      call("edu.emory.mathcs.restoretools.iterative.ParallelIterativeDeco
nvolution3D.deconvolveWPL", pathToBlurredImage, pathToPsf,
pathToDeblurredImage, boundary, resizing, output, precision, threshold,
maxIters, nOfThreads, showIter, gamma, filterXY, filterZ, normalize,
logMean, antiRing, changeThreshPercent, db, detectDivergence);
}
```

Supplemental Video

Click here to access/download

Supplemental Coding Files

Supplemental_Video_resubmission_538-3-P6-t2min-z750-xy143.66.avi